# Construction of a chiral metamaterial with a U-shaped resonator assembly

Xiang Xiong,[1] Wei-Hua Sun,[1] Yong-Jun Bao,[2,1] Mu Wang,[1,*] Ru-Wen Peng,[1,†] Cheng Sun,[2] Xiang Lu,[3] Jun Shao,[3] Zhi-Feng Li,[3] and Nai-Ben Ming[1]

[1]*National Laboratory of Solid State Microstructures, Department of Physics, Nanjing University, Nanjing 210093, China*

[2]*Department of Mechanical Engineering, Northwestern University, Evanston, Illinois 60208-3111, USA*

[3]*National Laboratory for Infrared Physics, Shanghai Institute of Technical Physics, Chinese Academy of Sciences, Shanghai 200083, China*

(Received 5 November 2009; published 23 February 2010)

In an assembly of double-layered metallic U-shaped resonators with two resonant frequencies $\omega_H$ and $\omega_L$, the effective induced electric and magnetic dipoles, which originate from the specific distribution of induced surface electric current upon the illumination of incident light, are collinear at the same frequency. Consequently, for left circularly polarized incident light, negative refractive index occurs at $\omega_H$, whereas for right circularly polarized incident light it occurs at $\omega_L$. We suggest that this design provides a new example to apply chiral structures to tune the electromagnetic properties, and could be enlightening in exploring chiral metamaterials.

DOI: 10.1103/PhysRevB.81.075119 PACS number(s): 42.25.Ja, 78.67.−n, 78.20.Ek, 73.20.Mf

Interaction of electromagnetic waves with subwavelength metallic microstructures has attracted much attention in recent decade due to the new physical properties and effects.[1–10] With specially designed metallic microstructures, it is possible to achieve novel electromagnetic properties that are not naturally available. One of the focused features nowadays is the negative refractive index, which was initially proposed as an academic concept by Veselago.[11] About three decades later, people found that it was possible to construct artificial structure to achieve a magnetic response.[12] Later on a composite structure based on split ring resonators was introduced and shown to have a frequency band over which the real parts of both permittivity ($\epsilon_r$) and permeability ($\mu_r$) are simultaneously negative, hence the negative refractive index was experimentally realized.[13] Up to now, metamaterial with negative refractive index has been realized with fishnets,[3,14] short wire pairs,[15,16] in addition to the split rings.[13,17]

An alternative way to achieve negative refractive index is to utilize chiral materials,[18–23] where the chirality suppresses the refractive index of light with one handedness, and increases the refractive index of light with the other handedness. Experimentally, chirality-induced negative refractive index has been demonstrated in cross-wire structure,[21] twisted rosettes,[22] and interlocked split-ring resonators.[24] It is especially interesting to note the terahertz chiral matematerial reported by Zhang *et al.*,[20] which is essentially a micro-sized inductor-capacitor (LC) resonance system. With this structure the electric and magnetic dipoles are strongly coupled and can be simultaneously excited. Further, the angle between the directions of effective electric and magnetic dipoles is relatively small, which contributes to an evident chiral behavior. We expect that once the angle between the directions of these two dipoles vanishes or equals to 180°, the chiral feature of the structure could be even more efficiently utilized.

In this paper we demonstrate that in an assembly of double-layered metallic U-shaped resonators (USRs), the effective induced electric and magnetic dipoles, which are contributed by the specific surface current distributions, are aligned in the same (or the opposite) direction at the same frequency. The resulted strong chiral feature leads to the negative refraction for circularly polarized light.

The geometry of double-layer-stacked USRs is schematically shown in Fig. 1(a), where the USRs on the upper layer and that on the lower layer have been orthogonally rotated. Similar to that in our earlier report,[25] the coordinate frame is so set that the diagonal directions of USRs are defined as $\boldsymbol{x}$ and $\boldsymbol{y}$ axes, respectively. Consequently, as shown in Fig. 1(a), the opening of the upper layer USR points to 45°, while that of the lower layer USR points to −45°. The geometrical parameters of USRs in Fig. 1(a) are $\boldsymbol{a}=4$ $\mu$m, $\boldsymbol{b}=1$ $\mu$m, and $\boldsymbol{g}=600$ nm. The thickness of each layer of U-shaped pattern is 100 nm. A commercial software based on the finite difference time domain (FDTD) method (CST Microwave Studio) is applied to calculate the transmission/reflection coefficients of the structure and to determine the induced surface electric current distribution. For normal incidence of electromagnetic wave ($z$-axis incidence), resonant dips occur at lower frequency $\omega_L$ ($\sim$390 cm$^{-1}$) and higher frequency $\omega_H$ ($\sim$590 cm$^{-1}$), respectively, as illustrated in Fig. 1(b). The distribution of the surface electric current at the frequencies of resonance has been calculated. At $\omega_L$, the electric currents on the upper and lower layers of USRs flow parallelly, whereas at $\omega_H$ the surface currents on the two layers are antiparallel, as illustrated in Figs. 1(c) and 1(d), respectively. It should be pointed out that the relative direction of the induced electric currents can be either parallel or antiparallel on two layers of USRs, and this feature is independent of the polarization of the incident light.

The induced electric current on the surface of metallic microstructures generates an induced electromagnetic field, which interacts with the incident fields and consequently leads to some novel optical properties. The effective induced surface electric current flowing on each layer of metal structure can be schematically plotted with the highlighted long arrows, as schematically shown in Figs. 1(c) and 1(d), respectively. The induced surface currents on the upper and the lower layers of USRs can be projected to $\boldsymbol{x}$ axis and $\boldsymbol{y}$ axis, respectively. At the lower resonant frequency $\omega_L$ [Fig. 1(c)],

 

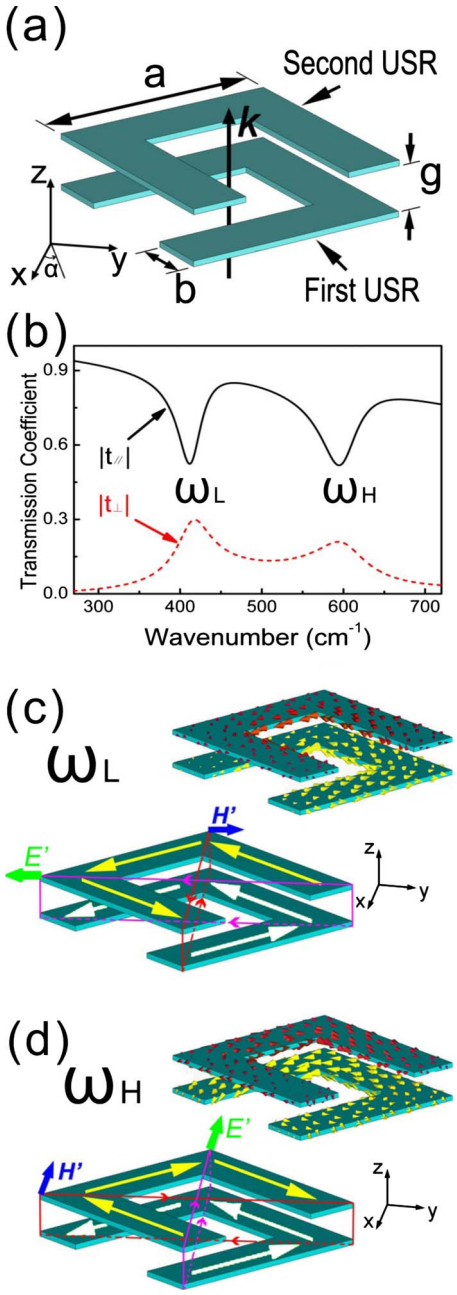


FIG. 1. (Color online) (a) The detail structure of the double-layered and orthogonally rotated USR pair with $\boldsymbol{a}=4.0$ $\mu$m, $\boldsymbol{b}=1.0$ $\mu$m, and $\boldsymbol{g}=0.6$ $\mu$m. The thickness of each U pattern is 100 nm. (b) The calculated transmission coefficient of USRs for normal incidence, and resonance occurs at $\omega_L$ and $\omega_H$. In the calculation the ambient is set as vacuum, and the polarization is along 45°. (c) and (d) The surface electric current density excited on USRs at lower ($\omega_L$) and higher ($\omega_H$) resonant frequencies. The small arrows represent the surface current distribution. By setting $\boldsymbol{x}$ and $\boldsymbol{y}$ axes along the diagonal directions of USRs, the surface current can be projected along $\boldsymbol{x}$ and $\boldsymbol{y}$ directions, respectively.

the projected currents along $\boldsymbol{x}$ axis on the upper and the lower layers are antiparallel. The projected currents on the upper and lower layers along $\boldsymbol{y}$ direction, however, are parallel. It follows that the curl integration along the loop in $x$-$z$ plane is nonzero, indicating that an induced magnetic filed

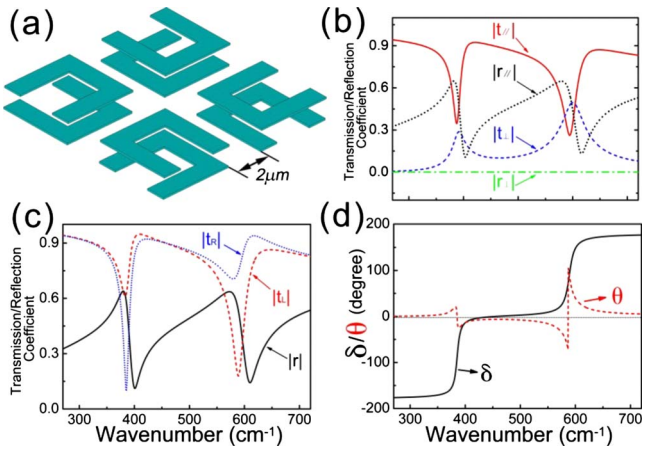


FIG. 2. (Color online) (a) The unit cell constructed by four pairs of USRs. The unit is arranged in a simple square lattice and the lattice parameter is 12 $\mu$m. (b) The amplitudes of $t_{\parallel}$, $t_{\perp}$, $r_{\parallel}$, and $r_{\perp}$. (c) The amplitudes of $t_L$, $t_R$, and $r$. (d) The diagram to show the phase difference $\delta$ between $t_{\perp}$ and $t_{\parallel}$ as a function of wave number, and the azimuth angle of the principal axis of polarization of transmission wave $\theta$ as a function of wave number.

$\boldsymbol{H}'$ is established along $\boldsymbol{y}$ direction (the Ampere's law), or, in other word, an effective magnetic dipole along $\boldsymbol{y}$ direction is induced. Along $\boldsymbol{y}$ direction, in $y$-$z$ plane, two parallel projected currents can be identified on the upper and the lower layers of USRs, suggesting that there is an induced electric filed $\boldsymbol{E}'$ along $\boldsymbol{y}$ direction (the Ohm's law), or, in other word, an effective electric dipole along $\boldsymbol{y}$ direction is induced. Similar analysis can be applied to surface current at higher resonance frequency $\omega_H$ [Fig. 1(d)], where an induced magnetic field $\boldsymbol{H}'$ occurs in $\boldsymbol{x}$ direction, and an induced electric filed $\boldsymbol{E}'$ occurs also in $\boldsymbol{x}$ direction. It should be noted that the induced magnetic fields in vertical direction $\boldsymbol{z}$ either cancel out (at higher resonance frequency $\omega_H$) or along the $k$ vector of the incident light (at lower resonance frequency $\omega_L$), and hence are not considered here.

In Fig. 1 the wave vector of the incident light is along $\boldsymbol{z}$ direction and the induced magnetic and electric dipoles are collinear along one of the diagonal directions ($\boldsymbol{x}$ or $\boldsymbol{y}$ axis) of USR, i.e., the effective induced electric and magnetic dipoles are parallel (or antiparallel), so their induced electric and magnetic fields are parallel (or antiparallel), allowing optical activity to occur more efficiently.

Four optically active USRs have been assembled into a unit with each USR separated 2 $\mu$m apart, as shown in Fig. 2(a). An array of such units arranged in simple square lattice has been constructed, and the lattice parameter equals to 12 $\mu$m. Due to the fourfold rotational symmetry of the unit, the transmission and reflection properties of this structure do not rely on the orientation of the sample with respect to the polarization of incident light. The structure shown in Fig. 2(a) is clearly different from what we reported early,[25] where the USRs as that shown in Fig. 1(a) ($U_1$) and its enantiomorphous counterpart ($U_2$) are used as building blocks to form an optically nonactive unit. In that kind of structure, the magnetic and electric responses can be switched at the same frequency by merely changing the polarization of the inci-

dent light.[25] For the structure made of the chiral units shown in Fig. 2(a), the FDTD software is applied to calculate the transmission and reflection coefficients, and the results are shown in Fig. 2(b). In the calculation, the permittivity of gold in the infrared regime is based on the Drude model, $\epsilon(\omega)=1-\omega_p^2/(\omega^2+i\omega_\tau\omega)$, where $\omega_p$ is the plasma frequency and $\omega_\tau$ is the damping constant. For gold, the characteristic frequencies are taken as $\omega_p=1.37\times10^4$ THz, and $\omega_\tau=40.84$ THz.[26] As shown in Fig. 2(b), two resonance dips occur at 390 and 590 $cm^{-1}$, respectively, which correspond to the transmission of parallel polarization of input and output light ($|t_\parallel|$) and to the transmission of perpendicular polarization of input and output light ($|t_\perp|$). For optically nonactive material, when the incident light is polarized along the principal axis (the axis along which the tensor of electric susceptibility is diagonal), only transmission of $t_\parallel$ could be detected and $t_\perp$ vanishes. However, for optically active material as we reported in this work, the chiral behavior helps to rotate the polarization of incident light and convert a portion of energy from one polarization to the other polarization. Hence $t_\perp$ will be detected.

Following the regulation, the transmission and reflection coefficients of the left-handed circularly polarized (LCP) light and the right-handed circularly polarized (RCP) light are expressed as $t_L=t_\parallel-it_\perp$, $t_R=t_\parallel+it_\perp$, $r_L=r_\parallel-ir_\perp$, and $r_R=r_\parallel+ir_\perp$, respectively. In our structure $r_\perp$ is zero [as shown in Fig. 2(b)], suggesting that the polarization of the reflection light does not change. The calculated transmission coefficients of LCP and RCP ($t_L$ and $t_R$) are shown in Fig. 2(c). Due to the chirality of the structure, the transmission for LCP and RCP split into two different curves [Fig. 2(c)]. Two resonant dips appear at $\omega_L=390$ $cm^{-1}$ and $\omega_H=590$ $cm^{-1}$ for both $t_L$ and $t_R$, respectively. For the resonance at $\omega_L=390$ $cm^{-1}$, the dip in $|t_R|$ is much deeper than that in $|t_L|$, suggesting that the resonance for RCP is much stronger than that for LCP. For the resonance at $\omega_H=590$ $cm^{-1}$, however, the dip of LCP is much deeper than that of RCP. We define $\delta$ as the phase difference between $t_\perp$ and $t_\parallel$. The dependence of $\delta$ as a function of wave number is illustrated in Fig. 2(d). It follows that an elliptical polarized light is generated[27] when $\delta\neq n\pi$ ($n$ is an integer). Meanwhile, the end of electric field vector revolves clockwise for sin $\delta>0$ and countclockwise for sin $\delta<0$. Consequently, the outgoing light below and above 460 $cm^{-1}$ (which corresponds to sin $\delta=0$) have different chirality. This fact also suggests that the resonances at lower and higher frequencies have different chirality. The azimuth angle of the principal polarization axis of the transmitted wave, $\theta$, is defined as $\theta=\frac{1}{2}[\arg(t_R)-\arg(t_L)]$.[21,27] It represents the change in polarization angle when a linearly polarized light is incident on the USR assembly. As plotted in Fig. 2(d), at $\omega_L$ the rotation angle reaches −25° and at $\omega_H$ the rotation angle reaches −72°.

It is known that the refractive indices for LCP and RCP lights can be expressed as[19] $n_{R/L}=\sqrt{\epsilon\mu}\pm\xi$, where $\epsilon$ and $\mu$ are the effective permittivity and permeability, respectively; $\xi$ describes the coupling between the electric and the magnetic dipoles along the same direction. Following Ref. 22, the effective impedance ($Z$) and refractive index for LCP and RCP light can be derived from the reflection and transmission coefficients and other material parameters

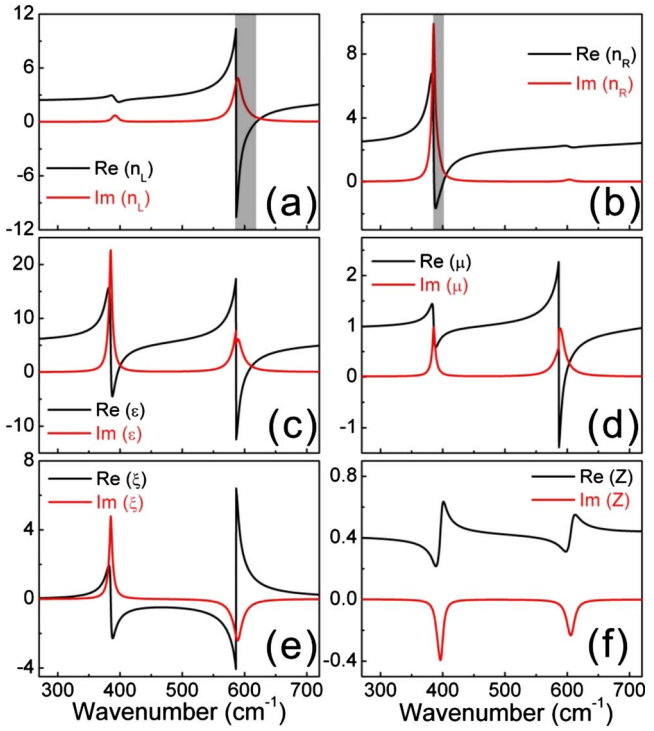


FIG. 3. (Color online) The retrieved effective optical parameters of USR arrays. (a) and (b) illustrate the real and imaginary parts of the refractive index for LCP and RCP light, respectively. The shadow denotes the occurrence of negative refractive index. (c)–(f) illustrate the real and imaginary parts of the permittivity $\epsilon$, permeability $\mu$, chiral parameter $\xi$, and the impedance $Z$.

$$\xi=(n_R-n_L)/2,$$

$$\mu=Z(n_R+n_L)/2,$$

$$\epsilon=(n_R+n_L)/2Z.$$

For our USR structures, evident drop of refractive index occurs at $\omega_H$ for LCP light [Fig. 3(a)] and at $\omega_L$ for RCP light [Fig. 3(b)]. Yet the refractive index shows much smaller modification for LCP beam at $\omega_L$ and for RCP at $\omega_H$. This is due to the cancellation of the contributions from the product of permittivity and permeability and that from the chirality. Far away from the resonant frequency, the difference between the refractive indices of RCP and LCP diminishes. The effective permittivity and permeability have been retrieved, as illustrated in Figs. 3(c) and 3(d). At $\omega_L$, the permittivity reaches negative values, whereas the magnetic resonance is not sufficiently strong to provide a negative permeability; at $\omega_H$ the modification of permittivity and permeability are both sufficiently strong, hence negative values are realized. The chiral term $\xi$ and impedance $Z$ are shown in Figs. 3(e) and 3(f), respectively, which demonstrate strong chirality of our USRs at both $\omega_L$ and $\omega_H$. Therefore, Fig. 3 demonstrates that the negative refractive index for LCP light around $\omega_H$ arises from two origins: one is from the negative value of both permittivity and permeability, and the other is from the

chirality of the structure ($\xi>0$). The negative refractive index for RCP light around $\omega_L$, however, originates only from the chirality ($\xi<0$). The efficiency of the negative refractive index is usually characterized by figure of merit (FOM), which is defined as FOM=$|\mathrm{Re}(n)/\mathrm{Im}(n)|$. For LCP light, we find that the negative refractive index at $\omega_H$ has FOM=2.4, while for RCP light, the negative refractive index at $\omega_L$ has FOM=2.5.

Based on the above calculations, we can get a type of chiral metamaterial with the array of units of fourfold rotated USRs. For normal incidence light, on each pair of USRs, parallel and antiparallel surface electric currents are excited on the upper and lower layers of USRs. Consequently, collinearly aligned effective electric dipole and an effective magnetic dipole are generated. These two dipoles are so strongly coupled at both $\omega_L$ and $\omega_H$ that they are simultaneously excited. It is this feature that leads to the optical activity. The effective induced electric and magnetic dipoles are aligned in the opposite direction at $\omega_L$ and in the same direction at $\omega_H$. This difference leads to the different handedness at the lower and the higher frequencies. It also contributes to the negative refractive index for RCP light or LCP light, respectively.

To check the above designing and calculations, the metallic array of units of fourfold rotated USRs is experimentally fabricated with alignment nesting photolithography. An array of negative U-shaped pattern is first defined on the substrate with photoresist. A 100-nm-thick gold film is then blanket deposited on the patterned substrate, covering the areas with photoresist and the areas where the photoresist has been removed (U-shaped pattern). Thereafter, the photoresist was removed with solvent, leaving only the gold USRs on silicon substrate. Then a layer of 600-nm-thick silicon nitride is deposited as a spacer layer. Thereafter, a layer of photoresist is once again spin coated, followed by alignment nesting lithography. The second layer of gold film (100 nm in thickness) is deposited and lift-off procedure is used to remove the photoresist, leaving only the second layer of gold USRs. During the fabrication, each USR on the upper layer located exactly above the one on the lower layer, yet the orientation had being rotated for 90° in a specific way. Consequently an array of specifically arranged chiral USR units is fabricated, as shown in Fig. 4(a). The inset of Fig. 4(a) shows the detailed morphology of the experimentally fabricated structure. For sake of structural symmetry in optical measurements, a 2-$\mu$m-thick silicon layer is cap deposited on the sample surface before finishing the sample fabrication.

The setup for optical measurements is schematically shown in Fig. 4(b). The chiral sample is characterized by a vacuum infrared Fourier-transform spectrometer (Bruker Vertex 70v). In the transmission measurement, the sample was placed between two linear polarizers, and angles $\theta_1$ and $\theta_2$ can be independently adjusted. Three sets of $T_\parallel$ and $T_\perp$ are measured with different $\theta_1$ and $\theta_2$. As shown in Fig. 4(c), the red (light gray) solid line corresponds to the scenario $\theta_1=\theta_2=-45°$; the blue (dark gray) solid line corresponds to the scenario $\theta_1=\theta_2=0°$; the black solid line corresponds to the scenario $\theta_1=\theta_2=45°$; the red (light gray) dash dot line corresponds to the scenario $\theta_1=-45°$ and $\theta_2=45°$; the black dash line corresponds to the scenario $\theta_1=45°$ and $\theta_2=-45°$;

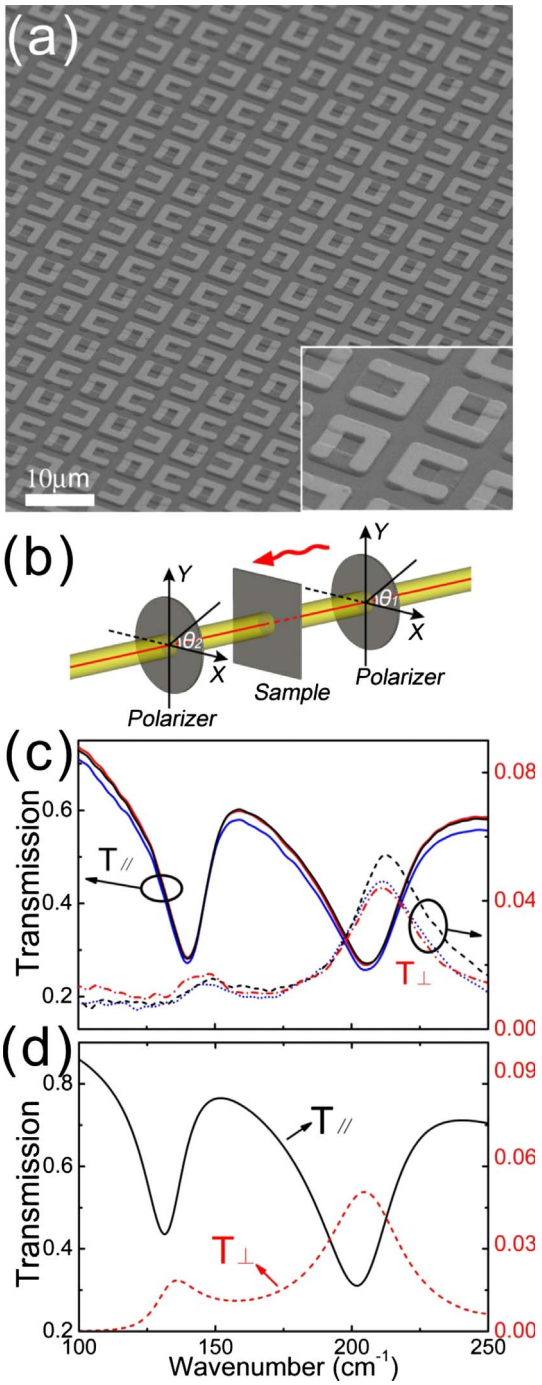


FIG. 4. (Color online) (a) The scanning electron micrograph of the double-layered USR arrays. The double-layer structure can be easily identified from the inset. (b) The schematics of the measurement setup. In the measurement, the arms of USRs are set in parallel with ***X*** and ***Y*** directions. The polarizer in front of and after the sample can be independently rotated with angle $\theta_1$ and $\theta_2$, respectively. (c) Experimentally measured transmission spectra with different polarizations of $\theta_1$ and $\theta_2$. The red (light gray) solid line: $\theta_1=\theta_1=-45°$; the blue (dark gray) solid line: $\theta_1=\theta_1=0°$; the black solid line: $\theta_1=\theta_1=45°$; the red (light gray) dash dot line: $\theta_1=-45°$ and $\theta_2=45°$; the black dash line: $\theta_1=45°$ and $\theta_2=-45°$; the blue (dark gray) dot line: $\theta_1=90°$ and $\theta_1=0°$. (d) Simulation of the transmission $T_\parallel$ and $T_\perp$. In simulation damping constant used in Drude model is doubled to fit the loss in real system.

and the blue (dark gray) dot line corresponds to the scenario $\theta_1=90°$ and $\theta_2=0°$, respectively. One may easily find out that all the $T_{\parallel}$ curves are almost identical and all $T_{\perp}$ curves are almost identical, suggesting that the transmission is polarization independent. Dips in $T_{\parallel}$ and peaks in $T_{\perp}$ at lower frequency (140 $cm^{-1}$) and higher frequency (205 $cm^{-1}$) indicate that at these two resonant frequencies, the USRs have rotated the polarization of light. It should be pointed out that for optical nonactive material, only transmission $T_{\parallel}$ could be detected and $T_{\perp}$ vanishes when the incident light is polarized along $\boldsymbol{x}$ or $\boldsymbol{y}$ axis. For our USR resonators, however, the chiral feature rotates the polarization of incident light and converts a portion of energy from one polarization to the other, which leads to the dips in $T_{\parallel}$ and the peaks in $T_{\perp}$. Simulations in Fig. 4(d) demonstrate excellent agreement with the experimental measurements.

The optical activity of chiral structures provides new approach to realize negative refractive index and has recently shown promising applications in designing new optical devices that may beat the diffraction limit,[6,28] and explore the highly sensitive sensors.[29,30] Thus far different types of chiral structures have been constructed,[20–22,31–36] and one of the important goals is to decrease the angle between the effective electric and magnetic dipoles, so to increase the efficiency in realizing negative refractive index. The USR structure reported here demonstrates a unique feature that the excited effective electric and magnetic dipoles are collinear. In this way, the chirality of our USRs can be fully utilized.

In conclusion, we report here a chiral structure made of an assembly of double-layered USRs, which produces negative refraction for LCP at $\omega_H$ and RCP at $\omega_L$. The chirality originates from the collinear excitation of effective electric and magnetic responses at the same frequency. The experimental data are in consistent with the calculations. Our current structure works in the infrared frequency, yet we expect that such principle should also work for other frequencies. We suggest that our design provides a new example to apply chiral structures in tuning the electromagnetic properties and could be enlightening in exploring chiral metamaterials.

The authors acknowledge the financial supports from Ministry of Science and Technology of China (Grants No. 2010CB630705 and No. 2006CB921804), NSF of China (Grants No. 10625417, No. 10874068, and No. 50972057), and Jiangsu Province (Grant No. BK2008012). The discussions with Xiang Zhang and Shuang Zhang are also sincerely acknowledged.

*muwang@nju.edu.cn
†rwpeng@nju.edu.cn

[1] J. B. Pendry, D. Schurig, and D. R. Smith, Science **312**, 1780 (2006).
[2] J. B. Pendry, A. J. Holden, W. J. Stewart, and I. Youngs, Phys. Rev. Lett. **76**, 4773 (1996).
[3] J. Valentine, S. Zhang, T. Zentgraf, E. Ulin-Avila, D. A. Genov, G. Bartal, and X. Zhang, Nature (London) **455**, 376 (2008).
[4] D. R. Smith, J. B. Pendry, and M. C. K. Wiltshire, Science **305**, 788 (2004).
[5] C. Genet and T. W. Ebbesen, Nature (London) **445**, 39 (2007).
[6] N. Fang, H. Lee, C. Sun, and X. Zhang, Science **308**, 534 (2005).
[7] E. Ozbay, Science **311**, 189 (2006).
[8] Y. J. Bao, R. W. Peng, D. J. Shu, Mu Wang, X. Lu, J. Shao, W. Lu, and N. B. Ming, Phys. Rev. Lett. **101**, 087401 (2008).
[9] C. M. Soukoulis, M. Kafesaki, and E. N. Economou, Adv. Mater. **18**, 1941 (2006).
[10] S. Linden, C. Enkrich, M. Wegener, J. F. Zhou, T. Koschny, and C. M. Soukoulis, Science **306**, 1351 (2004).
[11] V. G. Veselago, Sov. Phys. Usp. **10**, 509 (1968).
[12] J. B. Pendry, A. J. Holden, D. J. Robbins, and W. J. Stewart, IEEE Trans. Microwave Theory Tech. **47**, 2075 (1999).
[13] R. A. Shelby, D. R. Smith, and S. Schultz, Science **292**, 77 (2001).
[14] N. Liu, L. Fu, S. Kaiser, H. Schweizer, and H. Giessen, Adv. Mater. **20**, 3859 (2008).
[15] Z. F. Zhou, L. Zhang, G. Tuttle, T. Koschny, and C. M. Soukoulis, Phys. Rev. B **73**, 041101 (2006).
[16] G. Dolling, C. Enkrich, M. Wegener, J. F. Zhou, C. M. Soukoulis, and S. Linden, Opt. Lett. **30**, 3198 (2005).
[17] D. R. Smith, W. J. Padilla, D. C. Vier, S. C. Nemat-Nasser, and S. Schultz, Phys. Rev. Lett. **84**, 4184 (2000).
[18] S. Tretyakov, I. Nefedov, A. Sihvola, S. Maslovski, and C. Simovski, J. Electromagn. Waves Appl. **17**, 695 (2003).
[19] J. B. Pendry, Science **306**, 1353 (2004).
[20] S. Zhang, Y. S. Park, J. S. Li, X. C. Lu, W. L. Zhang, and X. Zhang, Phys. Rev. Lett. **102**, 023901 (2009).
[21] J. F. Zhou, J. F. Dong, B. N. Wang, T. Koschny, M. Kafesaki, and C. M. Soukoulis, Phys. Rev. B **79**, 121104 (2009).
[22] E. Plum, J. Zhou, J. Dong, V. A. Fedotov, T. Koschny, C. M. Soukoulis, and N. I. Zheludev, Phys. Rev. B **79**, 035407 (2009).
[23] C. Monzon and D. W. Forester, Phys. Rev. Lett. **95**, 123904 (2005).
[24] B. N. Wang, J. F. Zhou, T. Koschny, and C. M. Soukoulis, Appl. Phys. Lett. **94**, 151112 (2009).
[25] X. Xiong, W. H. Sun, Y. J. Bao, R. W. Peng, Mu Wang, C. Sun, X. Lu, J. Shao, Z. F. Li, and N. B. Ming, Phys. Rev. B **80**, 201105(R) (2009).
[26] M. A. Ordal, R. J. Bell, R. W. Alexander, L. L. Long, and M. R. Querry, Appl. Opt. **24**, 4493 (1985).
[27] J. D. Jackson, *Classical Electrodynamics* (Wiley, New York, 1999).
[28] N. Fang and X. Zhang, Appl. Phys. Lett. **82**, 161 (2003).
[29] I. A. I. Al-Naib, C. Jansen, and M. Koch, Appl. Phys. Lett. **93**, 083507 (2008).
[30] T. Driscoll, G. O. Andreev, D. N. Basov, S. Palit, S. Y. Cho, N. M. Jokerst, and D. R. Smith, Appl. Phys. Lett. **91**, 062511 (2007).
[31] E. Plum, V. A. Fedotov, and N. I. Zheludev, Appl. Phys. Lett. **93**, 191911 (2008).
[32] F. Miyamaru and M. Hangyo, Appl. Phys. Lett. **89**, 211105 (2006).
[33] A. Papakostas, A. Potts, D. M. Bagnall, S. L. Prosvirnin, H. J. Coles, and N. I. Zheludev, Phys. Rev. Lett. **90**, 107404 (2003).

[34] M. Kuwata-Gonokami, N. Saito, Y. Ino, M. Kauranen, K. Jefimovs, T. Vallius, J. Turunen, and Y. Svirko, Phys. Rev. Lett. **95**, 227401 (2005).
[35] M. Decker, M. W. Klein, M. Wegener, and S. Linden, Opt. Lett. **32**, 856 (2007).
[36] J. K. Gansel, M. Thiel, M. S. Rill, M. Decker, K. Bade, V. Saile, G. von Freymann, S. Linden, and M. Wegener, Science **325**, 1513 (2009).